Biomedical Optics EXPRESS

In situ structural and microangiographic assessment of human skin lesions with high-speed OCT

Cedric Blatter,[1] Jessika Weingast,[2] Aneesh Alex,[1] Branislav Grajciar,[1] Wolfgang Wieser,[3] Wolfgang Drexler,[1] Robert Huber,[3] and Rainer A. Leitgeb[1,*]

[1]*Center of Medical Physics and Biomedical Engineering, Medical University Vienna, Waehringer Guertel 18-20, 1090 Vienna, Austria*

[2]*Department of Dermatology, Division of General Dermatology, Medical University Vienna, Waehringer Guertel 18-20, 1090 Vienna, Austria*

[3]*Lehrstuhl für BioMolekulare Optik, Ludwig-Maximilians-Universität München, Oettingenstraße 67, 80538 Munich, Germany*

**rainer.leitgeb@meduniwien.ac.at*

Abstract: We demonstrate noninvasive structural and microvascular contrast imaging of different human skin diseases *in vivo* using an intensity difference analysis of OCT tomograms. The high-speed swept source OCT system operates at 1310 nm with 220 kHz A-scan rate. It provides an extended focus by employing a Bessel beam. The studied lesions were two cases of dermatitis and two cases of basal cell carcinoma. The lesions show characteristic vascular patterns that are significantly different from healthy skin. In case of inflammation, vessels are dilated and perfusion is increased. In case of basal cell carcinoma, the angiogram shows a denser network of unorganized vessels with large vessels close to the skin surface. Those results indicate that assessing vascular changes yields complementary information with important insight into the metabolic demand.

OCIS codes: (170.4500) Optical coherence tomography; (110.4500) Optical coherence tomography; (170.2655) Functional monitoring and imaging; (280.2490) Flow diagnostics.

References and links

1. K. Weidlich, J. Kroth, C. Nussbaum, S. Hiedl, A. Bauer, F. Christ, and O. Genzel-Boroviczeny, "Changes in microcirculation as early markers for infection in preterm infants--an observational prospective study," Pediatr. Res. **66**(4), 461–465 (2009).
2. T. Gambichler, V. Jaedicke, and S. Terras, "Optical coherence tomography in dermatology: technical and clinical aspects," Arch. Dermatol. Res. **303**(7), 457–473 (2011).
3. R. A. Leitgeb, "Current technologies for high speed and functional imaging with optical coherence tomography," in *Advances in Imaging and Electron Physics, Volume 168: Optics of Charged Particle Analyzers*, P. W. Hawkes, ed. (Elsevier, 2011), Chap. 3.
4. Y. Zhao, K. M. Brecke, H. Ren, Z. Ding, J. S. Nelson, and Z. Chen, "Three-dimensional reconstruction of *in vivo* blood vessels in human skin using phase-resolved optical Doppler tomography," IEEE J. Sel. Top. Quantum Electron. **7**(6), 931–935 (2001).
5. Y. Zhao, Z. Chen, C. Saxer, S. Xiang, J. F. de Boer, and J. S. Nelson, "Phase-resolved optical coherence tomography and optical Doppler tomography for imaging blood flow in human skin with fast scanning speed and high velocity sensitivity," Opt. Lett. **25**(2), 114–116 (2000).
6. Y. Zhao, Z. Chen, C. Saxer, Q. Shen, S. Xiang, J. F. de Boer, and J. S. Nelson, "Doppler standard deviation imaging for clinical monitoring of *in vivo* human skin blood flow," Opt. Lett. **25**(18), 1358–1360 (2000).
7. A. F. Fercher, C. K. Hitzenberger, G. Kamp, and S. Y. El-Zaiat, "Measurement of intraocular distances by backscattering spectral interferometry," Opt. Commun. **117**(1-2), 43–48 (1995).
8. R. Leitgeb, C. Hitzenberger, and A. Fercher, "Performance of fourier domain vs. time domain optical coherence tomography," Opt. Express **11**(8), 889–894 (2003).
9. M. Choma, M. Sarunic, C. Yang, and J. Izatt, "Sensitivity advantage of swept source and Fourier domain optical coherence tomography," Opt. Express **11**(18), 2183–2189 (2003).

#171698 - $15.00 USD Received 3 Jul 2012; rev. 30 Aug 2012; accepted 11 Sep 2012; published 24 Sep 2012

10. J. F. de Boer, B. Cense, B. H. Park, M. C. Pierce, G. J. Tearney, and B. E. Bouma, "Improved signal-to-noise ratio in spectral-domain compared with time-domain optical coherence tomography," Opt. Lett. **28**(21), 2067–2069 (2003).
11. G. Liu, W. Jia, V. Sun, B. Choi, and Z. Chen, "High-resolution imaging of microvasculature in human skin in-vivo with optical coherence tomography," Opt. Express **20**(7), 7694–7705 (2012).
12. J. Enfield, E. Jonathan, and M. Leahy, "*In vivo* imaging of the microcirculation of the volar forearm using correlation mapping optical coherence tomography (cmOCT)," Biomed. Opt. Express **2**(5), 1184–1193 (2011).
13. L. An, J. Qin, and R. K. Wang, "Ultrahigh sensitive optical microangiography for *in vivo* imaging of microcirculations within human skin tissue beds," Opt. Express **18**(8), 8220–8228 (2010).
14. J. Qin, J. Jiang, L. An, D. Gareau, and R. K. Wang, "*In vivo* volumetric imaging of microcirculation within human skin under psoriatic conditions using optical microangiography," Lasers Surg. Med. **43**(2), 122–129 (2011).
15. R. A. Leitgeb, M. Villiger, A. H. Bachmann, L. Steinmann, and T. Lasser, "Extended focus depth for Fourier domain optical coherence microscopy," Opt. Lett. **31**(16), 2450–2452 (2006).
16. A. Alex, B. Považay, B. Hofer, S. Popov, C. Glittenberg, S. Binder, and W. Drexler, "Multispectral *in vivo* three-dimensional optical coherence tomography of human skin," J. Biomed. Opt. **15**(2), 026025 (2010).
17. R. Huber, M. Wojtkowski, and J. G. Fujimoto, "Fourier domain mode locking (FDML): A new laser operating regime and applications for optical coherence tomography," Opt. Express **14**(8), 3225–3237 (2006).
18. C. Blatter, B. Grajciar, C. M. Eigenwillig, W. Wieser, B. R. Biedermann, R. Huber, and R. A. Leitgeb, "Extended focus high-speed swept source OCT with self-reconstructive illumination," Opt. Express **19**(13), 12141–12155 (2011).
19. A. Fullerton, M. Stücker, K.-P. Wilhelm, K. Wårdell, C. Anderson, T. Fischer, G. E. Nilsson, and J. Serup; European Society of Contact Dermatitis Standardization Group, "Guidelines for visualization of cutaneous blood flow by laser Doppler perfusion imaging. A report from the Standardization Group of the European Society of Contact Dermatitis based upon the HIRELADO European community project," Contact Dermat. **46**(3), 129–140 (2002).
20. E. B. Brown, R. B. Campbell, Y. Tsuzuki, L. Xu, P. Carmeliet, D. Fukumura, and R. K. Jain, "*In vivo* measurement of gene expression, angiogenesis and physiological function in tumors using multiphoton laser scanning microscopy," Nat. Med. **7**(7), 864–868 (2001).
21. A. Alex, J. Weingast, B. Hofer, M. Eibl, M. Binder, H. Pehamberger, W. Drexler, and B. Považay, "3D optical coherence tomography for clinical diagnosis of nonmelanoma skin cancers," Imaging Medicine **3**(6), 653–674 (2011).
22. D. Altamura, S. W. Menzies, G. Argenziano, I. Zalaudek, H. P. Soyer, F. Sera, M. Avramidis, K. DeAmbrosis, M. C. Fargnoli, and K. Peris, "Key points in dermoscopic diagnosis of basal cell carcinoma and seborrheic keratosis in Japanese," J. Am. Acad. Dermatol. **62**, 59–65 (2010).
23. J. Welzel, M. Bruhns, and H. H. Wolff, "Optical coherence tomography in contact dermatitis and psoriasis," Arch. Dermatol. Res. **295**(2), 50–55 (2003).
24. T. Gambichler, A. Orlikov, R. Vasa, G. Moussa, K. Hoffmann, M. Stücker, P. Altmeyer, and F. G. Bechara, "*In vivo* optical coherence tomography of basal cell carcinoma," J. Dermatol. Sci. **45**(3), 167–173 (2007).
25. J. M. Olmedo, K. E. Warschaw, J. M. Schmitt, and D. L. Swanson, "Optical coherence tomography for the characterization of basal cell carcinoma *in vivo*: a pilot study," J. Am. Acad. Dermatol. **55**(3), 408–412 (2006).
26. K. K. Lee, A. Mariampillai, J. X. Yu, D. W. Cadotte, B. C. Wilson, B. A. Standish, and V. X. Yang, "Real-time speckle variance swept-source optical coherence tomography using a graphics processing unit," Biomed. Opt. Express **3**(7), 1557–1564 (2012).
27. J. W. Baish and R. K. Jain, "Fractals and cancer," Cancer Res. **60**(14), 3683–3688 (2000).
28. B. J. Vakoc, R. M. Lanning, J. A. Tyrrell, T. P. Padera, L. A. Bartlett, T. Stylianopoulos, L. L. Munn, G. J. Tearney, D. Fukumura, R. K. Jain, and B. E. Bouma, "Three-dimensional microscopy of the tumor microenvironment *in vivo* using optical frequency domain imaging," Nat. Med. **15**(10), 1219–1223 (2009).
29. T. Schmoll, A. S. Singh, C. Blatter, S. Schriefl, C. Ahlers, U. Schmidt-Erfurth, and R. A. Leitgeb, "Imaging of the parafoveal capillary network and its integrity analysis using fractal dimension," Biomed. Opt. Express **2**(5), 1159–1168 (2011).

1. Introduction

Microcirculation imaging has the potential to play an important role in cancer diagnosis, therapy monitoring and for the development of antivascular treatments. Furthermore, various pathologies are known to affect the vascular network, some already at an early stage [1]. Qualitative and quantitative analysis of the vascular network might provide additional diagnostic information about the lesion and its pathogenesis. It requires a modality achieving resolution close to the size of a capillary blood vessel (~10 µm) over a large depth range in tissue (~1 mm) ideally noninvasively and with high-speed to keep the effects of motion artifacts low. Easy handling and operation would further support its clinical acceptance.

#171698 - $15.00 USD Received 3 Jul 2012; rev. 30 Aug 2012; accepted 11 Sep 2012; published 24 Sep 2012

Optical coherence tomography (OCT) is a promising candidate for imaging microvasculature *in vivo*. First it possesses important advantages as compared to alternative techniques: it is noninvasive, provides structural contrast with high resolution, and permits vascular contrast using exclusively the intrinsic motion property of flow. Furthermore, depth information is available and allows for assessment and segmentation of different layers of vascular beds.

The application of OCT to dermatology is generating rising interest because of the previously mentioned advantages. Several studies have already been conducted to investigate inflammatory skin diseases, such as dermatitis, or skin cancer, such as basal cell carcinoma [2]. They were however limited to the analysis of structural changes assessed from OCT intensity pictures alone. The capability of OCT to visualize also the vascular network has the capability to provide complementary information related to the important metabolic tissue demand.

Several techniques using OCT have been developed to contrast blood vessels [3] but few were applied to human skin microvasculature imaging *in vivo*. Although first 2D and 3D images of single vessels section have been presented already with time domain OCT [4–6], the limited acquisition speed prevented the measurement of larger vasculature patches. The development of Fourier domain OCT brought a dramatic increase in sensitivity which made *in vivo* full volume measurement with short acquisition time possible [7–10]. Human skin microcirculation imaging based on Fourier domain OCT was demonstrated by calculating the intensity-based Doppler variance [11]. An enhanced field of view (FOV) of up to 8 × 7 mm was shown by correlation mapping OCT [12]. Based on the method of Ultrahigh-Sensitive Optical Microangiography (UHS OMAG) [13] differences in the blood vessel network between normal skin and psoriatic skin conditions have been resolved [14].

High-speed is of paramount importance for *in vivo* imaging as it is virtually free of motion distortion. Furthermore it is advantageous for maintaining a lateral sampling to support the system resolution while flexibly selecting the optimal tomogram rate. Generally, the velocity sensitivity scales proportionally with the time delay between compared signals. This delay can be increased by processing successive tomograms taken at the same or close to same position as was shown in the papers cited above. Such time differences increase the sensitivity to even resolve capillary flow, however imaging becomes more sensitive to involuntary patient motion that leads to decorrelation of static tissue signals.

In this paper, we perform microcirculation imaging of skin using an extended focus OCT (xf-OCT) system [15]. xf-OCT that is based on Bessel beam illumination provides an enhanced depth of focus as compared to standard Gaussian illumination. Our system operates further at a center wavelength of 1300 nm for optimal penetration into skin tissue [16]. It is based on swept source OCT and provides high-speed imaging by employing a Fourier Domain Mode Locked (FDML) laser [17]. We demonstrate motion contrast imaging with high sensitivity by calculating the squared intensity difference between successive tomograms.

With this equipment we present microcirculation imaging of human skin lesions *in vivo*. For the first time, to the best of our knowledge, *in situ* and *in vivo* microvascularization of basal cell carcinoma of human patients is shown noninvasively with OCT. *In situ* assessment, meaning the examination of the lesion in the place where it occurs, is important because it provides unaltered information about the tissue perfusion and nutrition. Furthermore noninvasive *in vivo* measurement might allow in the near future on-site diagnosis as well as an efficient *in situ* guidance for the dermatologists of where to take biopsies.

#171698 - $15.00 USD Received 3 Jul 2012; rev. 30 Aug 2012; accepted 11 Sep 2012; published 24 Sep 2012

2. Methods

2.1. Setup

The optical setup (Fig. 1(a)) for extended focus OCT imaging is the same as the one previously published [18]. We remind here its main characteristics. It is a swept source based system equipped with a FDML laser centered at 1310 nm with a 140 nm full-bandwidth, giving an axial resolution of 12 µm in air. A buffering stage is used at the output of the swept source to achieve 220 kHz A-Scan rate. An axicon lens creates a Bessel intensity distribution that is relayed on the beam steering device and further in the objective back-focal plane to produce a Bessel beam illumination on the sample. Back-scattered light is collected by a path-decoupled Gaussian mode. The lateral point spread function of the system is thus a Gaussian apodized version of the Bessel beam. The lateral resolution can be evaluated from its $1/e^2$ lateral extend to be of ~15 µm, constant over an axial distance of ~500 µm. The interference signal is measured by a dual balanced detector (350 Mhz, PDB130C, Thorlabs) and further digitized at 500 MS/s using a data acquisition board with a 8 bit analog-to-digital converter (1 GS/s, ATS9870, Alazartech). The sensitivity of the system, evaluated by comparison with a standard system, is better than 100 dB. The measured sensitivity roll-off is −1.2 dB/mm. For skin imaging, an adapter plate containing a cover glass window of 150 µm thickness is centered on the lesion and then taped on the skin. Water is used as refractive index matching medium between skin surface and cover glass. The adapter plate is then fixed via a mating ring in front of the sample objective (L6) keeping the region of interest centered to the scanning beam (Fig. 1(b)).

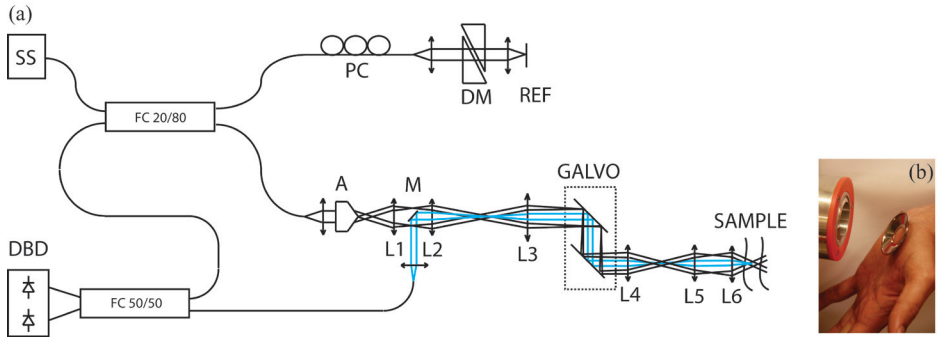

Fig. 1. (a) Optical Setup of the xf-OCT system. Blue: detection path. SS: Swept source, FC: Fiber coupler, PC: Polarization control, DM: Dispersion matching, A: Axicon, M: Mirror, L1 to L6: Lenses, Galvo: Scanning mirrors, DBD: Dual-balanced detector. (b) Adapter plate, containing a cover glass window, taped on a hand palm, in front of the mating ring that surrounds the objective lens on the left.

2.2. Microcirculation imaging

Highly motion-sensitive microcirculation imaging is performed by processing successive intensity tomograms. Intensity analysis has the advantage to be insensitive to electronic trigger jitter and thus to be well compatible with swept source OCT. An angiographic image volume *P*, contrasting flow against static tissue, is obtained by calculating the squared intensity difference between successive tomograms:

$$P(x,y_i,z)=\left(I(x,y_i,z)-I(x,y_{i+1},z)\right)^2, \qquad (1)$$

where $I(x,y,z)=20\cdot\log\left[\left|FFT(I(x,y,k))\right|\right]$, $(x,\ y,\ z)$ are the spatial pixel coordinates corresponding to fast and slow scanning and depth coordinate, respectively, and k is the wavenumber. Such method requires good correlation for static tissue over successive tomograms. This is obtained by driving the slow axis scanner with a multiple-step function. It

#171698 - $15.00 USD Received 3 Jul 2012; rev. 30 Aug 2012; accepted 11 Sep 2012; published 24 Sep 2012

allows for measuring N tomograms at the same position y. A calculation of the intensity squared difference mean value at each position permits to detect decorrelation, caused by motion artifact, and to potentially reject that picture for further processing by setting manually a threshold T. The value of T is chosen such as to obtain visually optimal vessel contrast. The pictures representing the same location can be averaged to increase SNR. The number of pictures averaged at each position can be formally written as

$$M(y) = \sum_{i=0}^{N-1} \left(\left[\sum_{x,z} P(x, y_i, z) \right] < T \right). \tag{2}$$

The logic operation in the brackets yields 1 or 0 for TRUE or FALSE, respectively. Finally, the motion contrast volume V is obtained by averaging only over the remaining M intensity squared difference tomograms P:

$$V(x, y, z) = \frac{1}{M(y)} \sum_{i=0}^{N-1} \left(\left[\sum_{x,z} P(x, y_i, z) \right] < T \right) \cdot P(x, y_i, z). \tag{3}$$

This method is more robust against motion artifacts than a variance analysis over the full tomogram series acquired at the same position, since pictures with strong decorrelation are rejected. Furthermore, the difference is only calculated between successive tomograms, thus reducing the time interval over which correlation is required. This improves further the stability with respect to motion artifacts.

3. Results

We recruited four patients with skin diseases: two affected by inflammation, and two by basal cell carcinoma. The microcirculation is compared to a representative healthy condition. The microvasculature reflects the health of the tissue and in particular its metabolic demand and its alteration should therefore exhibit a characteristic signature of the disease. In case of inflammation, we expect an increase in blood perfusion as has been previously demonstrated with Laser Doppler Imaging [19]. Basal cell carcinoma is expected to exhibit increased and chaotic vascularization through neoangiogenesis, as a result of the strong metabolic need due to uncontrolled cell growth. Such development of the vascular pattern has been demonstrated in animal studies [20].

In the following, microcirculation imaging was performed over a 2 × 2 mm FOV by acquiring N = 10 tomograms at 100 different vertical positions. The number of 10 tomograms is an empirical value selected such as to have on the one hand high microcirculation contrast and on the other hand enough data for motion contrast analysis after rejection of patient motion affected tomograms. In addition we aimed at keeping the measurement time as short as possible. Each tomogram contains 800 A-Scans. The acquisition was performed at 220 kA-Scans/s leading to a measurement time of about 4 seconds. In a second step, a highly sampled volume consisting of 800 tomograms, without any redundancy, was acquired.

The study was approved by the Ethics Committee of the Medical University of Vienna (EK-Nr: 1126/2009). Informed consent was given by all participants of the present study.

3.1. Healthy subject

The microvascularization of the palm of a healthy volunteer is used for indication of a normal condition. Figure 2(a) is a representative tomogram of the referred location visualizing the characteristic layers of a glabrous skin [21]. The stratum disjunctum (SD) appears as a first thin bright layer. It covers the thicker stratum corneum (SC) appearing as a low scattering layer. It contrasts with the viable epidermis (VE) that appears as a bright layer underneath. Its delineation with the papillary dermis (PD), region with lower scattering, is not a plane parallel to the surface but undulates, making a clear demarcation difficult. The reticular subpapillare (RS), visible as a dark line, separates the PD from the reticular dermis (RD) that appears as a

#171698 - $15.00 USD Received 3 Jul 2012; rev. 30 Aug 2012; accepted 11 Sep 2012; published 24 Sep 2012

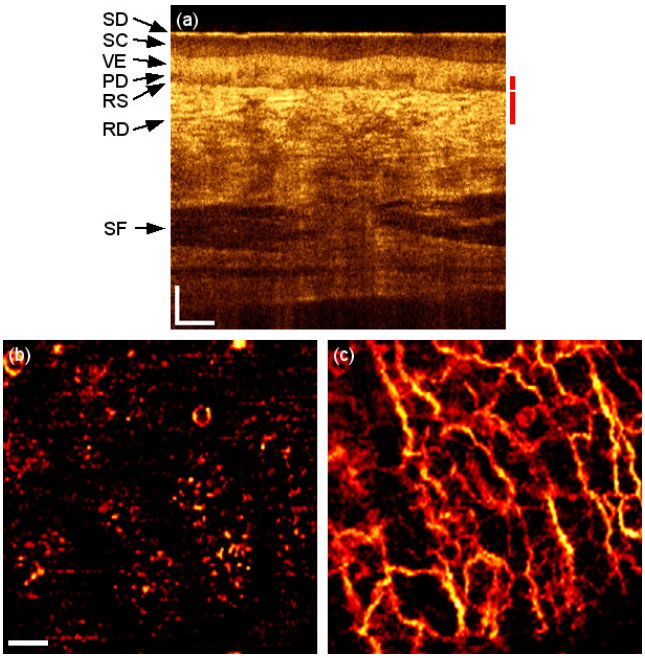

Fig. 2. Healthy skin of the palm. (a) OCT tomogram. Red bars indicate depth range for (b) and (c) respectively. SD: stratum disjunctum, SC: stratum corneum, VE: viable epidermis, PD: Papillary dermis, RS: Rete subpapillare, RD: reticular dermis, SF: subcutaneous fat. (b) and (c) 2 × 2 mm en-face mean projection over depth range indicated in (a) of the fly through the microvasculature starting from surface (Media 1). Scale bars indicate 250 µm in every picture.

bright area by the presence of a network of small blood vessels. Deeper, subcutaneous fat (SF) is visible. Figure 2(b) and 2(c) show the en-face microvascularization for two different depth ranges, 300 to 350 µm and 350 to 450 µm respectively. A mean projection is calculated over successive axial ranges in order to resolve two different kinds of vasculature: capillary loops feeding the living part of the epidermis, and a deeper planar vascular network that supports the capillary vessels. The vasculature images published in this paper are thresholded to reduce the background noise. This may however lead to missing signals visible as discontinuities along the contrasted vascular network.

3.2. Inflammation

The first patient suffers from allergy-induced eczema on the forearm (Fig. 3). A dermascope is used to acquire a reflectance picture of the lesion over a large FOV. Figure 3(a) shows the lesion and indicates the FOV of OCT. Dilated vessels and scaly patches are visible; however the resolution does not permit to resolve the finer vascular network. Furthermore no depth information is available. The OCT tomogram in Fig. 3(b) shows increased perfusion and vasculature visible through increased shadowing artifacts as compared to the healthy case. Also, the boundary between epidermis and dermis is less pronounced. The inflammation causes in general a smoother structure in the OCT tomogram of the dermis layer with fewer details as in the healthy case. An en-face mean projection of the highly sampled intensity volume is displayed in Fig. 3(c). Complementary information is provided by the OCT angiograms obtained with the squared intensity difference method. Figure 3(d) shows a microvasculature en-face mean projection image of the dermo-epidermal junction, displaying cross sections of superficial vertical capillary loops. The perfusion signatures of those capillaries are larger in diameter than those of the healthy control due to increased perfusion in the inflammation region. Relative change of perfusion can be inferred by our technique from visible vessel size changes. Also, the inflammation causes an alteration of the tissue

#171698 - $15.00 USD Received 3 Jul 2012; rev. 30 Aug 2012; accepted 11 Sep 2012; published 24 Sep 2012

structure that obviously leads to larger lateral distances between the capillary loops. The red areas in the dermascopy image are diagnosed as subcutaneous bleeding caused by scratching. It is expected that the blood visible with the dermascope should also be visible in the OCT tomogram because of the intrinsic stronger backscattering of blood. We observe in fact that the red areas of subcutaneous bleeding in the dermascopy image correlate well with the regions of enhanced backscattering seen in the OCT tomograms and marked with the asterisk in Fig. 3(b). Those areas do not appear in the motion contrast angiogram, since the subcutaneous blood is basically static. Figure 3(e) shows an overlay of the microcirculation on the structural information. Note that both pieces of information are extracted from the same data set, resulting in a perfect registration. The presented case is a nice example how complementary information given by structural as well as angiographic method helps for a better interpretation and understanding of the tissue pathology.

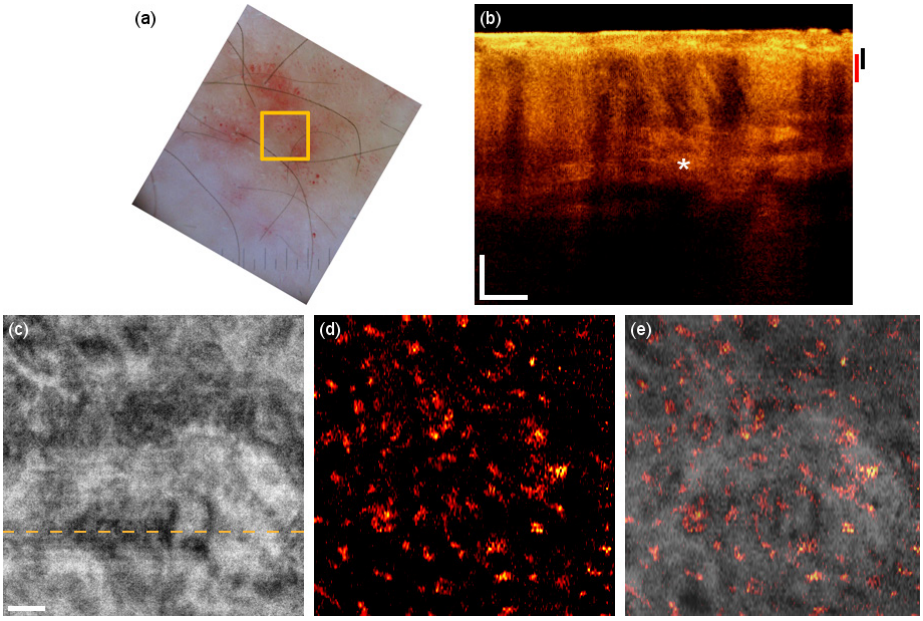

Fig. 3. Eczema on the forearm. (a) Dermascopy image with square indicating the OCT FOV. (b) OCT tomogram. Black and red bars indicate depth range for (c) and (d) respectively. (c) Intensity en-face mean projection for depth range in (b), dashed line indicates the tomogram position. (d) 2 × 2 mm en-face fly through the microvasculature starting from surface (Media 2). (e) Overlay of microcirculation on structural information. Scale bars indicate 250 µm in every picture.

A case of seborrhoeic dermatitis above the eyebrow is seen in patient 2 (Fig. 4). It is characterized by scaly, erythematous plaques, accompanied by physiologically closely spaced ducts of sebaceous and sweat glands. This condition is visible in the dermascopy image (Fig. 4(a)), as well as in the OCT pictures (Fig. 4(b) and 4(c)). The angiography in Fig. 4(d) shows increased perfusion as evident from the relatively large vessels at that particular depth surrounding the inflammation areas of the sebaceous and sweat glands. This is well visible in the overlay image in Fig. 4(e). The vessel structure that lies deeper in the tissue than the capillary loops shown in the previous case is obviously altered by the local circular inflammation areas. We believe that the patchy appearance of those vessels is due to strong flow velocity differences in combination with the thresholding procedure explained in section 2.2. Although the flow remains constant, the flow velocity changes due to the apparent changes in the vessel cross-sections. Again, the motion contrast image reveals the microcirculation supporting the pathologic regions that is neither visible from the dermascopy image nor from the OCT intensity information alone.

#171698 - $15.00 USD Received 3 Jul 2012; rev. 30 Aug 2012; accepted 11 Sep 2012; published 24 Sep 2012

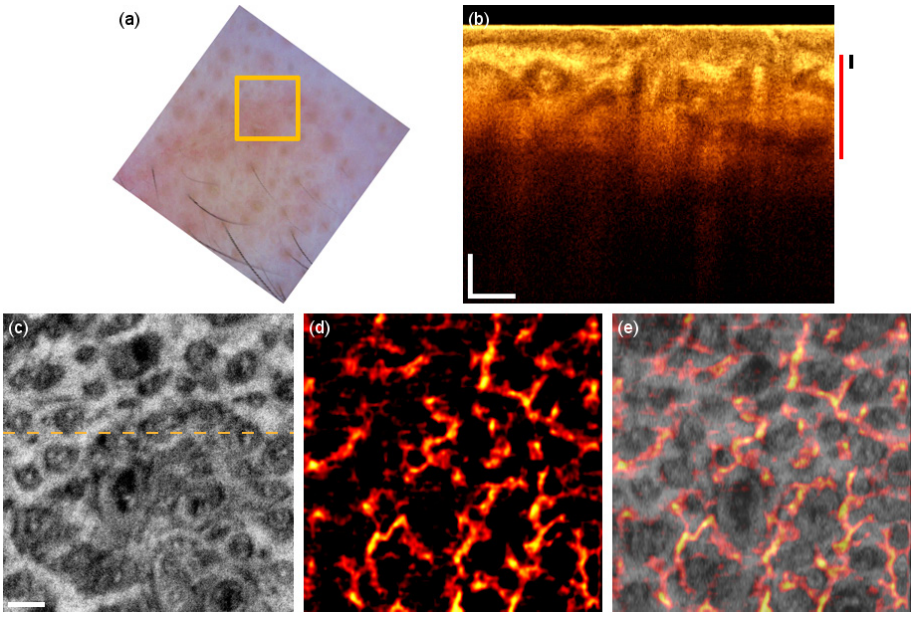

Fig. 4. Seborrhoeic dermatitis on the forehead. (a) Dermascopy image with square indicating the OCT FOV. (b) OCT tomogram. Black and red bars indicate depth range for (c) and (d) respectively. (c) Intensity en-face mean projection for depth range in (b), dashed line indicates the tomogram position. (d) 2 × 2 mm en-face fly through the microvasculature starting from surface (Media 3). (e) Overlay of microcirculation on structural information. Scale bars indicate 250 µm in every picture.

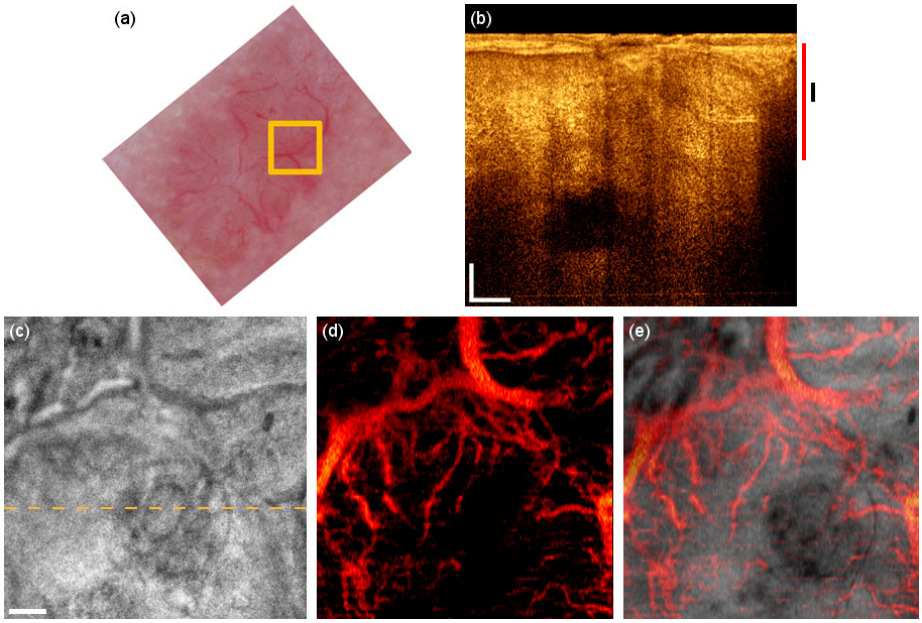

Fig. 5. BCC on the forehead. (a) Dermascopy image with square indicating the OCT FOV. (b) OCT tomogram. Black and red bars indicate depth range for (c) and (d) respectively. (c) Intensity en-face mean projection for depth range in (b), dashed line indicates the tomogram position. (d) 2 × 2 mm en-face fly through the microvasculature starting from surface (Media 4). (e) Overlay of microcirculation on structural information. Scale bars indicate 250 µm in every picture.

#171698 - $15.00 USD Received 3 Jul 2012; rev. 30 Aug 2012; accepted 11 Sep 2012; published 24 Sep 2012

3.3. Basal cell carcinoma

The third patient in the study suffers from basal cell carcinoma (BCC) on the forehead. Dermoscopy (Fig. 5(a)) reveals characteristic arborizing vessels, which are seen in 50-70% of BCCs [22]. The tomogram has a different signature, particularly in the epidermis region resembling the rolled border of the tumor caused by tumor cell aggregations surrounded by fibrous stroma (Fig. 5(b)). The dark areas in the deeper regions visible in the OCT tomogram are possibly necrotic or cystic regions. The OCT microvasculature imaging reveals a dense network of unorganized vessels (Fig. 5(d)). Furthermore, large vessels are abnormally present close to the surface. The large vessels branch out to provide the perfusion support through the smaller secondary vessels to the tumor sites with high metabolic demand.

Another case of BCC is present on the cheek of patient 4 (Fig. 6). The tomogram reveals a nodulo-cystic variant showing typical caviation due to degenerative changes (Fig. 6(b)). The vascular network seems denser on the right side of the en-face mean projection (Fig. 6(d)) leading to a bright area due to summation of perfusion signals in different depths. The vascular structure is better appreciated in the fly through movie (Media 5). The dark area on the lower left side of the motion contrast image is an indication of low perfusion. This could however be due to pressure of the glass plate visible as bright line to the sclerotic nodule in contact with the plate, which in turn obstructs the blood flow underneath. The vasculature in the fly-through movie shows again a chaotic vascular structure with large vessels and strong flow signatures. The isolated bright spot is an artifact caused by local strong sample reflection.

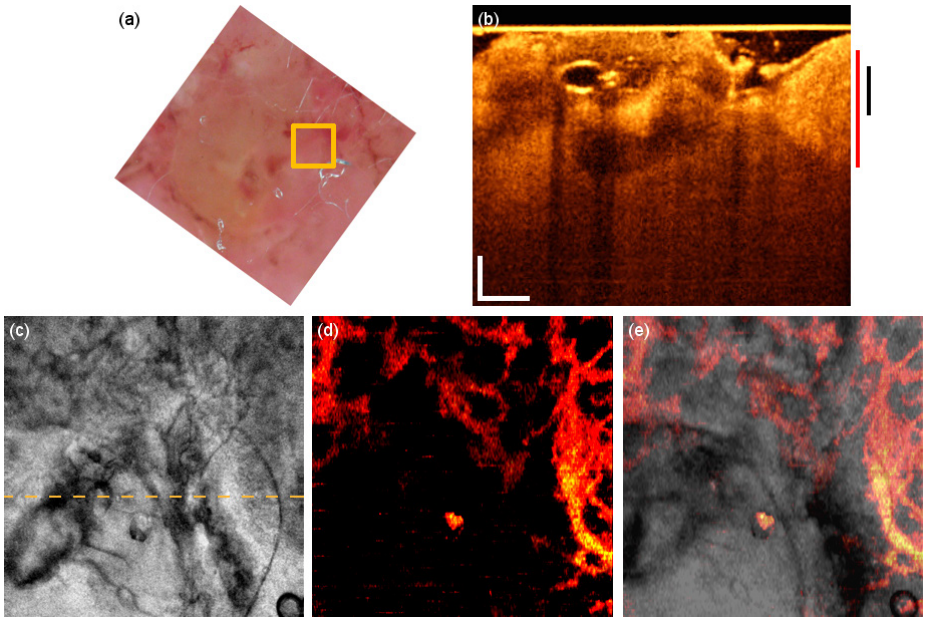

Fig. 6. BCC of the cheek. (a) Dermascopy image with square indicating the OCT FOV. (b) OCT tomogram. Black and red bars indicate depth range for (c) and (d) respectively. (c) Intensity en-face mean projection for depth range in (b), dashed line indicates the tomogram position. (d) 2 × 2 mm en-face fly through the microvasculature starting from surface (Media 5). (e) Overlay of microcirculation on structural information. Scale bars indicate 250 µm in every picture.

4. Discussion and conclusion

Concerning the intensity information, our findings on inflammation are in accordance with the work by Welzel et al. [23]. They outlined characteristic changes in the intensity OCT images: increase of dark areas being signal-free cavities in the dermis, partially due to dilated blood

#171698 - $15.00 USD Received 3 Jul 2012; rev. 30 Aug 2012; accepted 11 Sep 2012; published 24 Sep 2012

vessels, and less backscattering of the dermis with reduced demarcation to the epidermis. Also, the structural characteristics visible in the cases of BCC have been reported in previous studies. We observe a disorganization of the epidermis and the upper dermis structure [24] as well as increased backscattering in the surrounding stroma [25].

Due to our additional completely noninvasive motion contrast modality, we obtain further complementary information on the angiographic properties of the skin diseases. The measurements performed on different pathological conditions clearly indicate abnormal and characteristic signatures of the vasculature (see Table 1). In case of inflammation, increased perfusion signatures are present. In addition the capillary loops are enlarged and are more distant to each other. In case of BCC, the vasculature network is significantly altered. A denser network of unorganized vessels is visible with larger vessels in the superficial tissue regions. The larger vessels branch out and lead to secondary vessels that feed the tumor regions with high metabolic need. The comparison to the healthy skin yields certainly only a rough estimate of the pathologic condition, and further measurements with contrasting to vasculature in neighboring healthy regions or to that on a symmetric counterpart of the body are necessary. The main aim of this work was to emphasize and demonstrate the importance of having, in addition to high resolution structural OCT images, also the functional information as a diagnostically valuable complement at hand. Functional information as blood flow and vascular structure yields important insight into the metabolic demand of certain tissue pathologies, in particular of tumor regions.

Table 1. Comparison between the different pathological conditions

Condition	Effect on microcirculation
Healthy	Organized flat vessels beds with smaller capillary vessels in the upper layers and increased vessel size in deeper skin tissue.
Inflammation	Enlarged blood vessels, in particular capillaries, that indicate increased perfusion.
Basal cell carcinoma	Denser network of unorganized vessels with chaotic branching; larger vessels even close to the skin surface; capillary structure less pronounced and visible.

Our method provides noninvasive imaging of microvasculature at high-speed. A short acquisition time is required for artifact free *in vivo* imaging, particularly when patients, who have difficulties maintaining a stable position, are measured. *In vivo* and *in situ* assessment, meaning a measurement at the location where a pathological condition is detected, provides, without surgical intervention or preparation, unaltered information about the lesion and its natural perfusion and nutrition environment. It is a step towards noninvasive on-site diagnosis that might provide an efficient guidance for the dermatologists of where to take biopsies. This could eventually reduce the number of excised biopsies and improve patient comfort.

We decided to use intensity difference analysis for vascular imaging because firstly we avoid trigger jitter problems, and secondly, the computation is rather fast for providing sufficient contrast to distinguish between healthy and pathological conditions. The capability of GPU based real time speckle variance imaging has in fact been recently demonstrated [26]. Intensity based methods do not need calculation intensive bulk motion correction algorithms as do phase sensitive approaches. However, as they detect changes of the intensity signal, they are prone to artifacts due to changing illumination especially in regions of strong backscattering, or in cases of specular reflexes. A general disadvantage of highly sensitive motion contrast techniques is the decorrelation signal appearing below vessels that reduce the axial vessel segmentation. This is not visible in en-face mean projections but can reduce the quality of 3D rendering. The Bessel geometry helps to slightly reduce those artifacts [18].

We believe that our imaging method is applicable for treatment monitoring by providing information on antivascular treatment effectiveness, in case of photodynamic therapy for example. This imaging technique could also be used to assess the stage of the disease not only qualitatively but also quantitatively. Analysis on vessel density or the fractal dimension of the

#171698 - $15.00 USD Received 3 Jul 2012; rev. 30 Aug 2012; accepted 11 Sep 2012; published 24 Sep 2012

vascular tree can potentially give more precise information about the severity and progression of the disease [27–29].

A larger FOV would certainly ease the diagnosis and shorten the measurement session. Local changes in the vascularization pattern might be found within a single acquisition. The FOV is currently limited by the scanning system that is designed to yield a virtual common scanning pivot point for both scanning coordinates. Also, aberrations need to be kept small over the scanning angle to maintain a proper Bessel beam illumination.

In conclusion we demonstrated the performance of our extended focus high-speed OCT system to image the vascular system of healthy and of diseased skin with comprehensive details. The speed helps to minimize motion artifacts for *in vivo* measurements, which in addition results in better functional contrast. The various vascular patterns observed may lead to improved differentiation of healthy from diseased skin, but could also lead to the identification and diagnosis of skin diseases in deeper layers that are not visible from the dermascopy image alone. Furthermore, the density, integrity, and branching structure of the visualized vascular system may be valuable parameters to grade the stage of diseases, to monitor treatment progression, guide biopsies, and to uniquely give insight into the metabolic demand of the tissue.

Acknowledgments

We acknowledge financial support from the European Commission Seventh Framework Programme (FP7) HEALTH program (grant 201880, FUN OCT). Branislav Grajciar is funded by the Austrian Christian Doppler Association. We thank Thomas Klein, Benjamin R. Biedermann and Christoph M. Eigenwillig for their kind support with the FDML source.

#171698 - $15.00 USD Received 3 Jul 2012; rev. 30 Aug 2012; accepted 11 Sep 2012; published 24 Sep 2012